Spiral Beacon Calibration and Experiments for Underwater Localization

Rúben S. Viegas*, Friedrich Zabel†, João Gomes* and António Silva‡
*Institute for Systems and Robotics/LARSyS, Instituto Superior Técnico, Universidade de Lisboa, Lisboa, Portugal
†Marsensing Lda, Faro, Portugal
‡CISCA, Universidade do Algarve, Faro, Portugal
Emails: ruben.viegas@tecnico.ulisboa.pt; fredz@marsensing.com; jpg@isr.tecnico.ulisboa.pt; asilva@ualg.pt

***Abstract*—Underwater localization and navigation are still challenging tasks due to the underwater acoustic channel characteristics. Spiral sources are underwater transducers that create structured acoustic fields from which the angle to the source can be readily obtained. The angle estimation is obtained from the phase difference between transmitted circular and spiral fields, but for reliable operation the transducers must be properly calibrated. This paper presents a spiral source calibration procedure with the integration of a stepper motor to measure phase and amplitude features of the transmitted circular and spiral fields, at multiple bearing angles. The calibration was performed for two developed prototypes, which in turn determined the most appropriate operating frequency range. For one of the prototypes, its linearity was confirmed at all the tested frequency ranges through homogeneity and additivity tests. In addition to calibration, acoustic localization experiments were carried out with the transmission of circular and spiral fields, with a comparative analysis against footage captured from the top of the test pool. The phase difference of the mobile hydrophone was subtracted to the phase difference of the reference hydrophone to compute the angle between the spiral beacon and the mobile hydrophone. The localization results revealed noteworthy angular errors, hypothesized to be associated with the Doppler effect induced by the movement of the mobile hydrophone. These calibration and localization experiments suggest that spiral sources could be an important enabling technology for safe and reliable localization of underwater vehicles.**

***Index Terms*—Spiral Source, Underwater Acoustics, Transducer Calibration, Underwater Localization**

I. Introduction

The exploration of spiral acoustic fields in underwater environments has seen remarkable progress in recent years, presenting unique applications in underwater navigation [1], [2] and target detection SONAR [3]. Research advancements have highlighted the efficacy of spiral acoustic fields, offering a promising alternative to traditional methods in underwater applications that, typically, rely on measuring the time of flight (TOF) of the acoustic signal to perform localization, using multiple omnidirectional hydrophones or/and projectors, such as long baseline (LBL) [4], short baseline (SBL) [5], ultra-short baseline (USBL) [6], and networking techniques [7]–[9].

For a correct operation of spiral-field methods, it is necessary to emit a spiral field and a circular field. The spiral field exhibits a linear phase shift concerning the bearing angle, while the circular field maintains a constant phase along the bearing angle. The circular field is emitted to nullify phase changes caused by the environment, working as a reference field. The direction of the acoustic source can be estimated using the phase difference of the two fields in a similar way to the very high frequency omnidirectional range (VOR) technique. The employment of these fields for localization stands out for its simplicity, requiring only a single source/hydrophone pair for direction determination without reliance on time of flight [2], [10].

Typically, a spiral acoustic source comprises multiple acoustic elements oscillating with distinct phases, a design methodology exemplified in prior research [10]–[14]. Alternatively, these fields can be created through the vibration of a spiral-shaped surface, termed as the "Physical-Spiral" approach [11], [15]. While both techniques yield spiral fields, the physical-spiral method tends to be narrowband in nature, unlike the phased-spiral approach, which exhibits broader bandwidths [15].

Two prototypes of spiral acoustic sources were developed (Fig. 1), with the same principle described in [10] but with piezoelectric ceramics with larger diameters (54 and 51 mm). This change reduces the resonance frequencies and, consequently, the produced sound is less attenuated as it propagates through water. The ceramics used to manufacture the transducers are STEMINC PZT-4 piezoelectric cylinder with part numbers SMC5447T40111 and SMC5145T14111, which, based on their dimensions and material properties, are expected to have a circular resonance frequency of 17 kHz and 22 kHz, respectively. Based on this characteristic, the prototypes were named 17k and 22k, respectively. The spiral resonance frequency is expected to occur at 24 kHz and 31 kHz, respectively, based on the vibration modes mentioned in [3], [10].

In this work, the two prototypes were calibrated and one of them was used to locate a mobile hydrophone (spiral beacon experiment). In Section II, the two experiment setups used in this work are described. In Section III, the calibration experiments are presented, and, in Section IV, the localization experiments using a spiral beacon are described. Finally, in Section V, the conclusion and future work are presented.

(a)

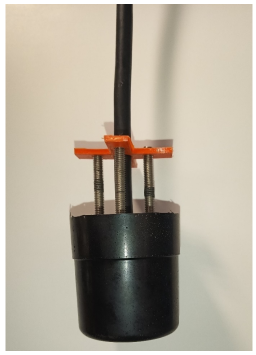

(b)

Fig. 1: The developed prototypes of spiral acoustic sources: **(a)** 17k and **(b)** 22k, with theoretical circular resonance frequency of 17 kHz and 22 kHz, respectively, and with theoretical spiral resonance frequency of 24 kHz and 31 kHz, respectively.

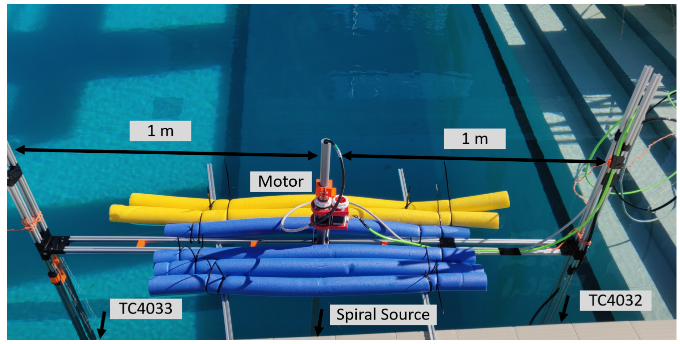

Fig. 2: Stepper Motor structure with the Spiral Source and the hydrophones TC4033 and TC4032. In the center, on the surface, there is a stepper motor that is connected to the spiral source so that it rotates when desired.

II. Experiment Setups

The experiments were carried out in a 16 by 16 meter pool with 4.3 meters depth. The Spiral Source Calibration experiment (Section III) was performed in two different setups: Stepper Motor Setup and Underwater Container Setup. The Spiral Beacon Underwater Localization experiment (Section IV) was performed with the Underwater Container Setup. Both Experiment Setups are described.

A. Stepper Motor Setup

The Stepper Motor Setup consisted of placing the structure represented in Fig. 2 in the center of the pool. In the center of the structure, the spiral source, at 1.3 m depth, was connected to a stepper motor on the surface. Two calibrated and static hydrophones (RESON TC4033 and TC4032) were placed on opposite ends of the structure at one meter from the spiral source and at the same depth. The stepper motor is computer-controlled through a wired connection, and, in this way, the rotation of the motor allows the spiral source to rotate, and the acoustic signals are acquired at the hydrophones for different bearing angles of the spiral source.

The electronic setup for generating and acquiring the transmitted and received signals was the same used in [10]. The transmitted signals were digitally generated using a computer and sent to the USB-1208HS-4AO DAQ for digital-to-analog conversion. Four toroidal transformers with unity-gain were employed to guarantee the electrical isolation between the four quadrants prior to applying the signals to the spiral source. On the receiving end, a USB-1602HS-2AO DAQ in differential mode was used to receive the signal collected by the TC4032, and a 42 dB gain pre-amplifier was used to acquire the signal in a different USB-1602HS-2AO DAQ in single-ended mode by the TC4033. The transmitted signal in Quadrant B of the spiral source was also obtained by the latter DAQ, which was utilized as a synchronization signal. All signals were acquired with a sample rate of 1 Msps.

In a similar way to [10], [16], sequences of linear up-chirps, with duration of 0.8 ms and a frequency bandwidth of 500 Hz, with center frequencies from 10 kHz to 50 kHz, with a step of 2.5 kHz, were emitted simultaneously in the four quadrants of the spiral source. The initial chirp phase of the transmitted chirps for the circular field is 0 degrees in the four quadrants, and for the spiral field is 0, 90, 180, and 270 degrees in quadrants A, B, C, and D, respectively. A sequence corresponds to the emission of several circular fields followed by spiral fields, where the frequency of the fields increases. The chirp duration and the silence between fields was 0.8 ms and 49.2 ms, respectively. Before and after the sequence of linear up-chirps, a synchronization chirp was also transmitted in the four quadrants. A synchronization chirp is a linear up-chirp from 10 kHz to 50 kHz, with initial chirp phase of 0 degrees, duration of 3.2 ms and later silence of 46.8 ms. The amplitude of the transmitted signals was 0.75 V and 4 V for the spiral sources 17k and 22k, respectively.

After the sequence transmission, the signals are acquired at the hydrophone output and the direct paths of the acoustic signals are extracted based on the channel estimation using the synchronization chirps [10]. The direct path signal due to the circular field and the one due to the spiral field will be termed $r(t)$ and $s(t)$, respectively.

The transmission and reception of acoustic signals was carried out sequentially, for both prototypes, for 25 uniformly distributed motor angles. Emissions were carried out with the static system and after the motor rotates, a pause is made to ensure that there is no additional noise during emissions.

B. Underwater Container Setup

The Underwater Container Setup consists of placing the spiral source 17k and a reference hydrophone (Hydrophone TC4032) at the bottom of the pool so that they are as static as possible. For this, the structure shown in Figure 3 was used, which contains the spiral source 17k, the Hydrophone TC4032 and an underwater container. The Spiral Source was placed at 1.37 m from the bottom and the hydrophone at 1.3 m from the bottom. The distance between the two devices is 1 meter. The quadrant A of the spiral source was facing the hydrophone.

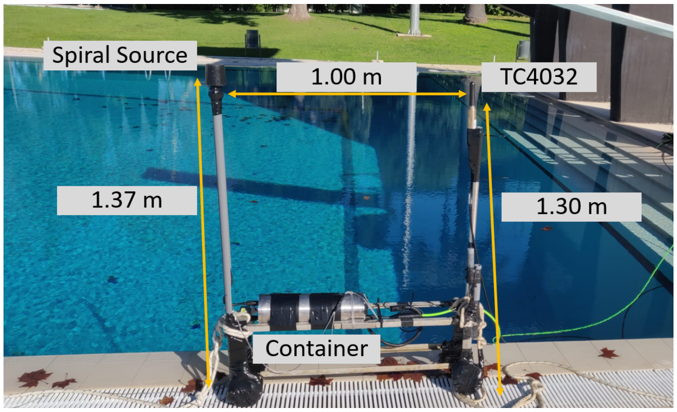

Fig. 3: Underwater Container structure with the Spiral Source (in the left), and the hydrophone TC4032 (in the right). In the center, on the bottom, there is the underwater container connected to the spiral source for the signal transmission.

The underwater container has (i) a microcontroller, controlled via Ethernet, which generates the transmission signals, (ii) four power amplifiers and (iii) four toroidal transformers for amplification and impedance adaptation. The full amplification system has a gain of 34 dB.

In this setup, the hydrophone TC4033 was placed 2.08 m from the surface, attached to a separate floating structure for mobility. This structure was used for the Spiral Beacon Underwater Localization experiment (Section IV).

On the receiving end, a USB-1602HS-2AO DAQ is used to acquire, in single-ended mode, the signals from the Hydrophones TC4033 and TC4032. The signals from the Hydrophone TC4033 were amplified by a 42 dB gain pre-amplifier. All signals were acquired with a sample rate of 1 Msps.

III. Spiral Source Calibration

The calibration of underwater transducers is crucial for correct operation of the respective systems. A spiral source should be calibrated to determine the operation frequency range and to determine the phase misalignments at different frequencies. Furthermore, it is important to perform a homogeneity and additivity test to determine at which frequencies the spiral source is approximately linear [16]. Although the calibration procedures have already been described in [10], [16] with manual rotations of the spiral source, in this work a stepper motor was used to increase the angular resolution of the calibrations. The results of Sections III-A and III-B were obtained with the Stepper Motor setup and the results of Section III-C with the Underwater Container setup.

A. Transmitting Voltage Response

The Transmitting Voltage Response (TVR) characterizes the pressure amplitude generated, per Volt, at 1 meter, by an acoustic source over a frequency range. The TVR of the spiral source for each frequency f_c can be computed, with all quantities in dB, by

$$\mathrm{TVR}(f_c) = V_{\mathrm{OUT}}(f_c) - \mathrm{OCVR}(f_c) - \mathrm{PA} - V_{\mathrm{IN}}, \quad (1)$$

where V_{OUT} is the received signal amplitude, OCVR is the calibrated hydrophone's Open Circuit Voltage Response (OCVR), PA is the pre-amplifier gain, and V_{IN} is the input signal amplitude. Regarding the electronic setup, the pre-amplifier gain for the TC4033 and TC4032 was 42 dB and 0 dB, respectively.

Figure 4 shows the computed TVR of the two prototypes (17k and 22k) acquired on both hydrophones at a bearing angle of 0 degrees. Fig. 4a indicates that the circular and spiral field resonances of the 17k spiral source occurs at approximately 15 kHz and 22.5 kHz, respectively, and are close to the theoretical values: 17 kHz and 24 kHz. In addition to the indicated resonances, it is possible to identify the longitudinal vibration mode resonance of piezoelectric ceramic, that occurs at approximately 37.5 kHz in both the circular field and the spiral field. Its theoretical value is 42 kHz based on the height of the ceramic and the PZT-4 properties. Fig. 4b indicates that the circular and spiral field resonances of the 22k spiral source occur at approximately 22.5 kHz and 30 kHz, respectively, and are close to the theoretical values: 22 kHz and 31 kHz.

Figure 5 shows the computed TVR of the two prototypes (17k and 22k) acquired on hydrophone TC4032 at 25 different bearing angles, also called horizontal directivity. Figure 5a shows the horizontal directivity of the 17k spiral source at its resonance frequencies (15 kHz and 22.5 kHz), and Figure 5b shows the horizontal directivity of the 22k spiral source at its resonance frequencies (22.5 kHz and 30 kHz). With the exception of the spiral TVR at 15 kHz in the 17k spiral source, all TVR curves have a circular appearance which indicates approximately constant power in all horizontal directions, as desired. The irregular shape of the spiral TVR at 15 kHz in the 17k spiral source may be due to the low SNR of the received signals caused by the low TVR.

At frequencies higher than the spiral resonance frequency, the TVR curves begin to lose their circular shape, probably because the ceramic does not vibrate radially at these frequencies. The maximum TVR variations across the bearing angle are around 15.5 dB and 4.6 dB for the 17k and 22k spiral sources, respectively.

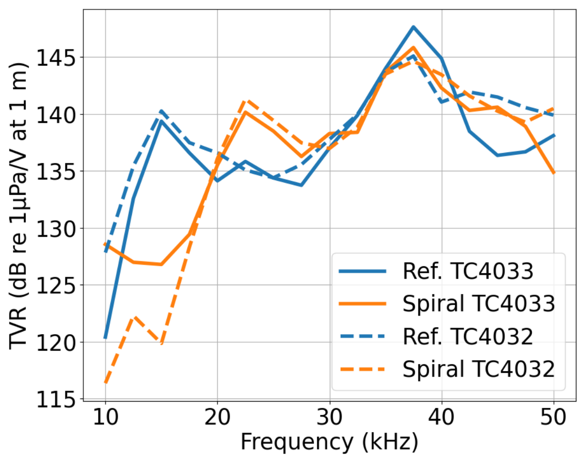

(a)

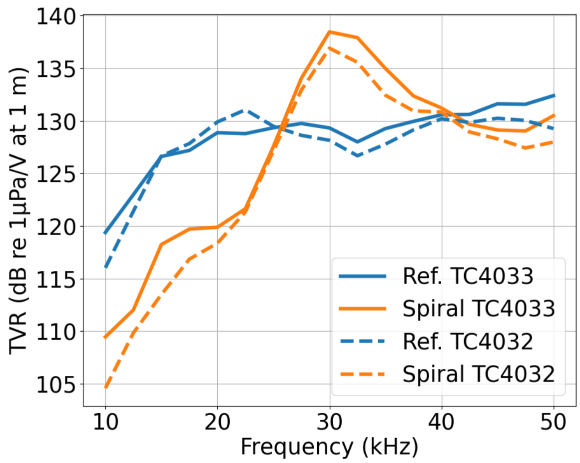

(b)

Fig. 4: TVR of the circular/reference field (blue lines) and spiral field (orange lines), for both hydrophones, for: **(a)** the 17k spiral source, and **(b)** the 22k spiral source.

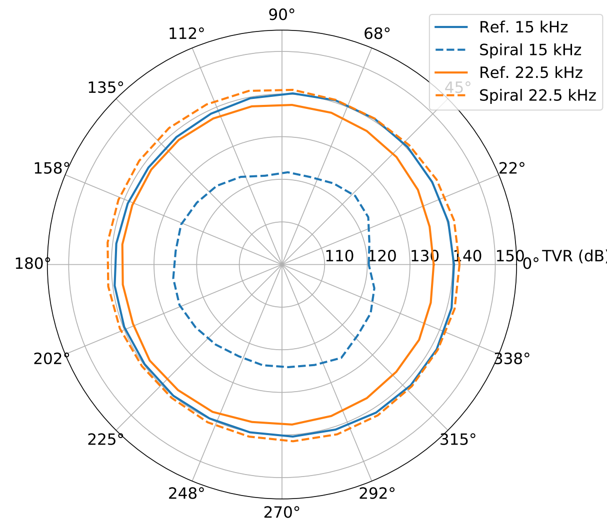

(a)

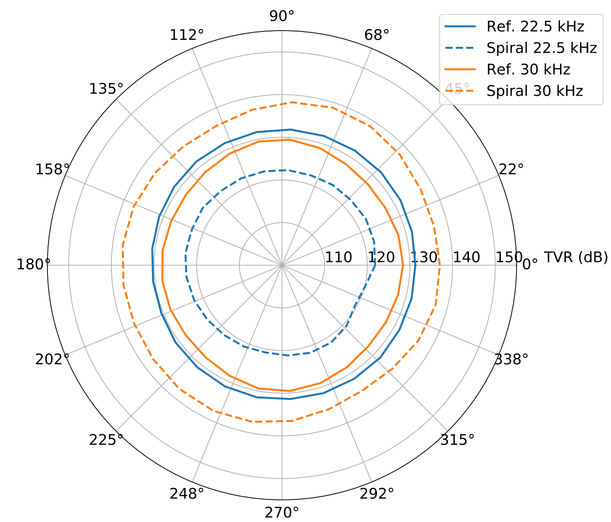

(b)

Fig. 5: Horizontal Directivity for the reference/circular and spiral field transmission at the resonance frequencies for: **(a)** 17k spiral source, and **(b)** 22k spiral source.

B. Phase Difference between Circular and Spiral Fields

The phase difference between the two signals (reference/-circular and spiral), at the center frequency f_c, is given by

$$\Delta\phi(f_c, \theta) = B\left[\arg\left(S(f_c)\right) - \arg\left(R(f_c)\right)\right], \qquad (2)$$

where $R(f)$ and $S(f)$ are the Fourier transforms of the received $r(t)$ and $s(t)$ signals, respectively, $B[]$ is a phase wrapping that confines the angle to the range $[-\pi; \pi[$, arg() is the complex argument function, and θ is the spiral source bearing angle relative to the hydrophone.

Figure 6 shows the polar plot of phase differences for different bearing angles for the two spiral sources (17k and 22k). The radial dimension represents the signal frequency. The solid and dashed lines represent the phase differences based on the signals from hydrophone TC4033 and TC4032, respectively. The values of all acquired angles are not shown to avoid cluttering the figures.

By analyzing Figures 6a and 6b it is possible to confirm that a spiral field is generated in both prototypes because the phase difference at each bearing angle has a constant offset relative to neighbouring angles. The constant offset corresponds to the motor rotation. On the other hand, there are large variations in phase difference across frequency, which must be accounted for to correctly estimate bearings. Furthermore, it is possible to observe that in the 17k spiral source there is greater variability between the hydrophones at frequencies above 30 kHz, which corresponds to its spiral resonance frequency. This high phase difference variability may be related to the nonlinearity of the transmission electronics, or related to the nonlinearity the spiral source at these frequencies. This should be analyzed further.

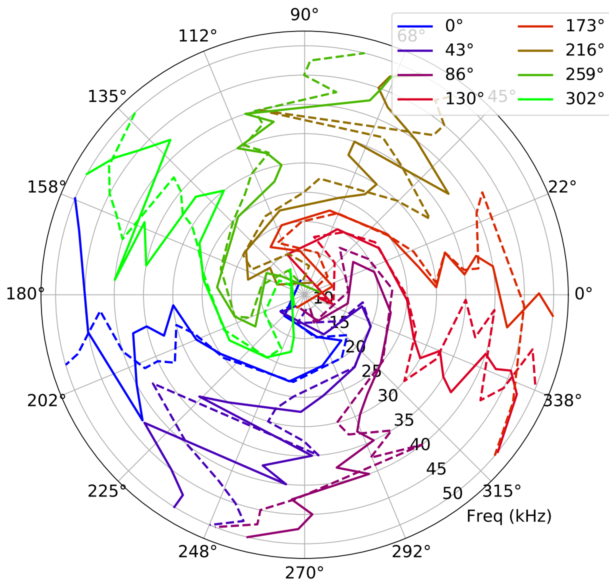

(a)

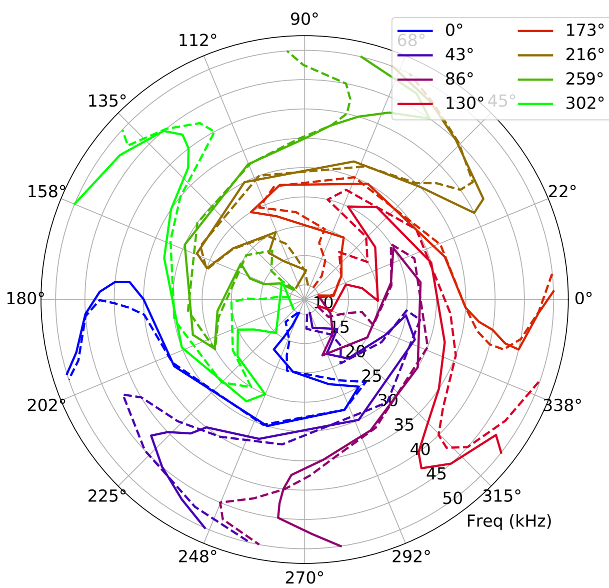

(b)

Fig. 6: Polar plot of the phase differences for different bearing angles for the prototypes: **(a)** 17k and **(b)** 22k. The radial dimension represents the signal frequency. The solid and dashed lines represent the phase differences based on the signals from hydrophone TC4033 and TC4032, respectively.

C. Linearity Evaluation

The linearity evaluation aims to test whether the quadrants of the spiral source are in accordance with the equation

$$\mathrm{T}\left(\sum_{q=A}^{D} \alpha_q x_q(t)\right) \stackrel{?}{=} \sum_{q=A}^{D} \alpha_q \mathrm{T}\left(x_q(t)\right), \tag{3}$$

where $T()$ is the transformation of the emitted signals, α_q is a multiplicative constant for quadrant q, and $x_q(t)$ is the signal emitted in quadrant q. For a system to be linear, the system must be homogeneous and additive [16].

To test homogeneity and additivity, it is necessary to ensure that the transmission system provides sufficient current so that non-linear effects do not occur, distorting the signal and reducing its amplitude. For this purpose, the linearity tests were carried out with the Underwater Container Setup (Section II-B) in which the electronic components are adapted for the spiral source 17k. Due to the non-guarantee of linearity of the associated electronics connected to the spiral source 22k, evaluation of its linearity was deferred to future work.

The homogeneity test consisted of transmitting 12 times the same sequence of signals with different input amplitudes: 0.1 V, 0.2 V, 0.4 V, and 0.8 V. The sequence of signals used in this case was a sequence of linear up-chirps with duration of 1.0 ms and a frequency bandwidth of 500 Hz, with center frequencies from 10 kHz to 50 kHz, with a step of 2.5 kHz. For each center frequency a circular and a spiral chirp were transmitted, with 50 ms of silence between them.

The following were calculated for the TC4032 received signals: (i) the TVR for the two types of fields (circular and spiral); and (ii) the phase difference between the two fields. Figures 7a and 7b show the mean TVR values and the mean phase differences, respectively, as well as their standard deviations. Except for 0.8 V signals, the TVR values and phase differences remain consistently similar across various amplitudes, indicating that the TVR and phase of the spiral source are independent of signal amplitude. Signals with 0.8 V amplitude were transmitted after carrying out other experiments, so there may have been changes in positioning of some of the devices that slightly affect the bearing angle. Despite this detail, the results strongly support the view that the spiral source 17k is a homogeneous system.

Comparing values in Figure 4a and Figure 7a reveals a reduction of approximately 6 dB in circular and spiral TVR at higher frequencies. This reduction is attributed to the use of a low-pass filter in the signal generation system at the underwater container. Furthermore, the frequency of the maximum spiral TVR of Figure 7a (25 kHz) is closer to the expected 24 kHz mentioned in Section I.

To test additivity, the sequence of transmitted signals needed to be changed. The additivity sequence, for a given center frequency, starts with the emission of a circular field, followed by a spiral field (in the following these are termed as "simultaneous signals", because in both cases all four quadrants are driven at the same time); and then the circular and spiral signals of each quadrant are emitted separately (in the following termed as ”separate signals”, because only one quadrant is driven at a time). The parameters of the chirps and synchronization chirps are the same as for the homogeneity assessment. An additivity sequence was transmitted and received 12 times for each central frequency used in the calibration.

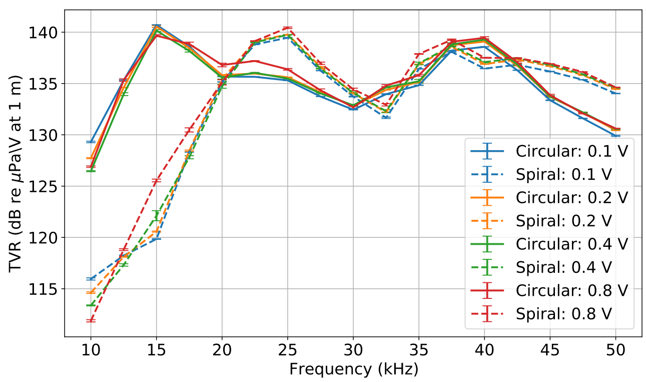

(a)

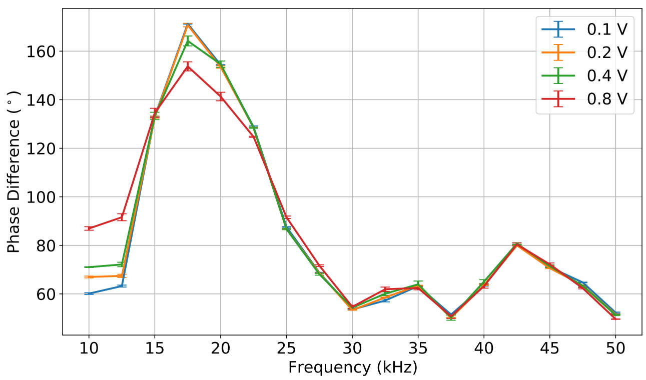

(b)

Fig. 7: Homogeneity test: **(a)** mean TVR and **(b)** mean phase difference values measured using the TC4032 hydrophone, for emitting amplitudes of 0.1 V, 0.2 V, 0.4 V, and 0.8 V. The vertical error-bars show the standard deviation.

After isolating the direct paths of the received signals, the signals from each quadrant are summed and compared with the simultaneous signal. This process was done for the circular wavefront and for the spiral wavefront. From now on, the signal obtained by summing the four signals from each quadrant is termed separate signal.

In order to compare the amplitude and phase of the two signals (simultaneous and separate), two metrics were used to evaluate the additivity of the spiral source over frequency, in four different positions: Relative Error Percentage of Amplitude, and Absolute Phase Difference. The first metric is given by

$$\epsilon_A = 100\,\frac{|A_{\text{simul}} - A_{\text{sep}}|}{A_{\text{simul}}}, \tag{4}$$

where A_{simul} and A_{sep} are the amplitudes of the simultaneous and separate signals, respectively, that were obtained from the Fourier transform of the signals. The Absolute Phase Difference is the absolute value of (2).

Figure 8 shows the Relative Error Percentage of Amplitude, and Phase Difference for the prototype 17k based on the signals from hydrophone TC4032. The values of both metrics are the mean values over 12 repetitions for the same bearing angle (corresponding to quadrant A). For all of the frequencies tested, the values of Relative Error Percentage of Amplitude and Phase Difference are lower than 15% and 8°, respectively, indicating that the systems are approximately additive.

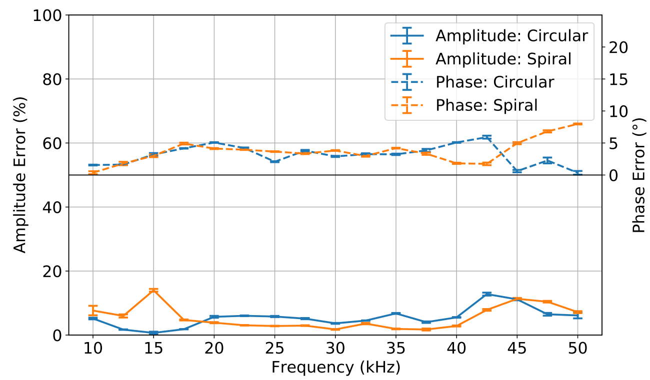

Fig. 8: Relative Error Percentage of Amplitude and Phase Difference between the circular or spiral field, and the sum of the signals from each quadrant for the spiral source 17k. The values of both metrics are obtained from 12 repetitions for the same bearing angle (corresponding to quadrant A).

The additivity and homogeneity results show that, for the experimental frequency range, the spiral source 17k behaves like a linear system for the bearing angle corresponding to quadrant A. Due to TVR frequency dependency, it is suggested to operate the spiral source 17k between 15 and 25 kHz for higher efficiency, which corresponds to the expected theoretical range. Since the transducer is linear, the variability of the phase difference between hydrophones represented in Figure 6a is probably due to the electronics used on the Stepper Motor Setup (Section II-A), but this requires confirmation.

IV. Spiral Beacon Underwater Localization

After calibrating the spiral sources, experiments were carried out to locate a mobile hydrophone (Hydrophone TC4033), using the Underwater Container Setup (Section II-B). The mobile hydrophone was placed at different positions around the pool with the spiral source 17k in the center and at the bottom of the pool. Thus, the spiral source works as a spiral beacon because it is static and it is used by receiving devices to self-localize.

For this experiment, in addition to the synchronization chirps at the beginning and end, a sequence of linear up-chirps was transmitted. The chirps have a duration of 2.0 ms and a frequency bandwidth of 500 Hz, with center frequencies of 15.0 kHz, 17.5 kHz, 20.0 kHz, and 22.5 kHz. For each center frequency, a circular and a spiral chirp were transmitted.

The silence between chirps was 100 ms, and the full signal sequence was transmitted in loop during all the experiment (approximately 14 minutes).

Contrary to the Stepper Motor Setup, the spiral source input signals cannot be directly recorded, so the delay synchronization must be obtained from the reference hydrophone (Hydrophone TC4032). Since the hydrophone TC4032 was located one meter from the spiral beacon, the distance between the spiral beacon and the mobile hydrophone, $\widehat{r}$, can be given by

$$\widehat{r} = 1 + c\left(\tau_m - \tau_0\right), \tag{5}$$

where c is the underwater sound speed (1473.0 m/s from CTD measurements), τ_m is the signal delay of the mobile hydrophone and τ_0 is the signal delay of the reference hydrophone. Furthermore, the reference hydrophone can also be used to automatically calibrate the system if the spiral source has not been calibrated. In this work, this case is considered, so the direction of the mobile hydrophone relative to the spiral beacon, $\widehat{\theta}_m$, is computed based on the phase difference of the reference and mobile hydrophones, $\Delta\phi_0$ and $\Delta\phi_m$, respectively, and is given by

$$\widehat{\theta}_m\left(f_c\right) = \Delta\phi_m\left(f_c, \theta_m\right) - \Delta\phi_0\left(f_c, \theta_0\right) + \theta_0, \tag{6}$$

where f_c is the center frequency of the received signals, θ_m and θ_0 are the true angles between the spiral source and the mobile and reference hydrophones, respectively. At the used setup $\theta_0 = 0°$. Considering that the spiral source is at the origin of the complex plane, the estimated position of the mobile hydrophone, $\widehat{\lambda}$, based on the proposed acoustic method, is given by

$$\widehat{\lambda} = \widehat{r}e^{j\widehat{\theta}_m}. \tag{7}$$

The location of the mobile hydrophone on the surface throughout the experiment was filmed from a springboard at a height of 10 m. The surface position of the mobile hydrophone relative to the pool borders was then obtained using image processing techniques. The actual position of the mobile hydrophone, λ, based on a given video frame, can be given by

$$\lambda = re^{j\theta}, \tag{8}$$

where r is the distance, in meters, between the spiral beacon and the mobile hydrophone that is given by

$$r = \sqrt{d^2 + r'^2}, \tag{9}$$

where d is the vertical distance between the spiral beacon and the mobile hydrophone (0.85 meters), r' is the top-view distance between the spiral beacon and the mobile hydrophone, given by

$$r' = \alpha\sqrt{\left(x_h - x_c\right)^2 + \left(y_h - y_c\right)^2}, \tag{10}$$

where α is the pixel scale (0.0205 meters per pixel), (x_h, y_h) is the hydrophone position and (x_c, y_c) is the spiral beacon position, both in pixels. θ is the direction of the hydrophone, in radians, given by

$$\theta = \text{atan2}\left(y_h - y_c, x_h - x_c\right). \tag{11}$$

Figure 9 shows one example frame from the top-view recorded video after perspective compensation. The green and red circles represent the surface position of the mobile hydrophone and the spiral source, respectively. The spiral source position was estimated based on an orange floater placed between the spiral source and the reference hydrophone attached to the container structure.

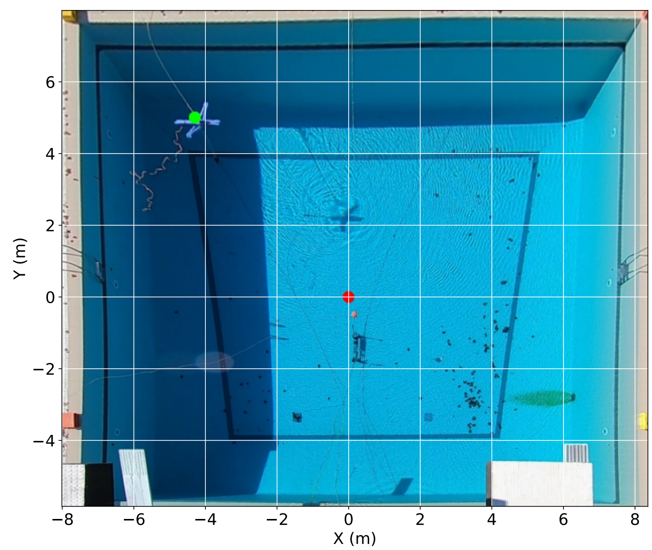

Fig. 9: Example Frame from the top-view video recorded during the experiment. The green and red circles represent the surface position of the mobile hydrophone and the spiral source, respectively.

Figure 10 shows the comparison between acoustic and visual localization. Figure 10a shows the distances between the mobile hydrophone and the spiral source: r and $\widehat{r}$. In fact, the temporal correlation between these two quantities was used to synchronize the acoustic dataset with the visual dataset. The results show that most of the time the distances are close, with the exception of two moments: [0, 250] and [650, 830] seconds. In these moments larger distance errors occur, probably due to the tilt of the mobile hydrophone structure when it is being pulled.

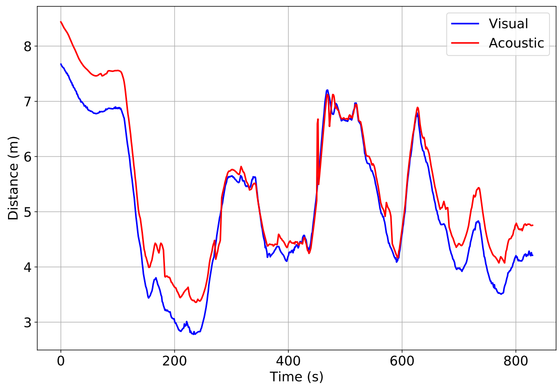

(a)

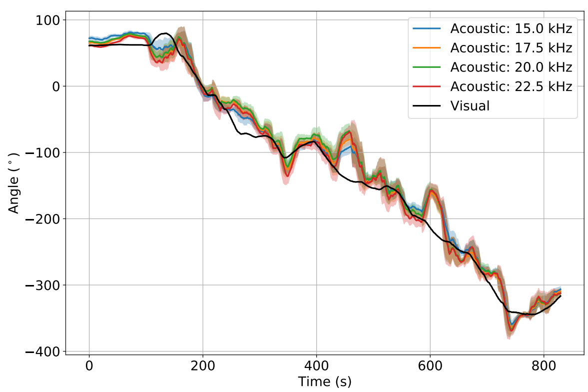

(b)

Fig. 10: Comparison between acoustic and visual localization: **(a)** distance comparison, and **(b)** angle comparison. In **(b)**, the acoustic curves presented are the angle after filtering with a phase-wrapped moving average with a window size of 13 samples. The shaded uncertainty region corresponds to the phase-wrapped standard deviation of the circular moving average samples.

Figure 10b shows the angles between the mobile hydrophone and the spiral source: θ and $\widehat{\theta}_m$ at the four tested center frequencies. The acoustic curves presented are the angle after filtering with a phase-wrapped moving average with a window size of 13 samples. The shaded uncertainty region corresponds to the phase-wrapped standard deviation of the phase-wrapped moving average samples. The estimated values using the acoustic method are reasonably close to the angle obtained visually, but significant differences remain. This phenomenon may be related to the Doppler effect due to the movement of the mobile hydrophone.

The radial velocity, v_r, between two instants of time (t_0 and t_1) can be computed based on the video frame information and is given by

$$v_r = \frac{r\left(t_1\right) - r\left(t_0\right)}{t_1 - t_0}. \tag{12}$$

Figure 11 shows the absolute radial velocity of the mobile hydrophone computed with (12) and the absolute angular error (absolute value of the difference between the visual and acoustic angles) for the 22.5 kHz estimations, for example. The values of the acoustic angles are the angle values after applying the moving average mentioned previously. The plot shows a strong relation between the two quantities, suggesting that the Doppler effect caused by the mobile hydrophone must be compensated, as suggested in [2]. Without this compensation, the angular error reaches up to 70°.

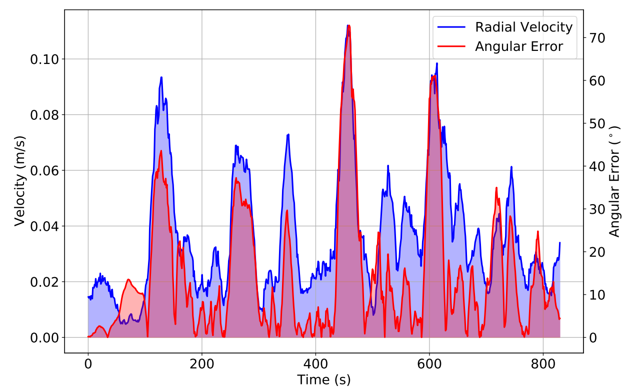

Fig. 11: Absolute radial velocity of the mobile hydrophone and the absolute angular error for the 22.5 kHz estimations over the experiment time.

V. Conclusion

This worked examined a promising solution for underwater localization and navigation using spiral acoustic sources. A spiral source calibration procedure was described and the respective results were presented for the two developed prototypes. The stepper motor system was able to increase the calibration resolution that is important to improve the underwater localization using spiral fields by characterizing its amplitude and phase characteristics more accurately. For one of the prototypes (prototype 17k), its linearity was confirmed at all the tested frequency range through homogeneity and additivity tests.

The localization of a mobile hydrophone through the emission of circular and spiral fields was also studied. This localization method was compared with footage taken from the top of the test pool. The localization results showed noteworthy angular errors, probably due to the Doppler effect caused by the movement of the mobile hydrophone. These localization experiments provide further experimental evidence that spiral fields are a promising method for underwater acoustics.

In future work, ideally, calibration with the stepper motor should be done with the hydrophones at a distance of more than 1 meter to reduce motor rotation errors. Regarding the location experiment, the angle localization should be calculated using calibration data, as in [10], instead of the phase difference to a reference hydrophone. In this way, the underwater location system only requires a single source/hydrophone pair. Finally, the Doppler effect must be compensated, which requires a study of the best methods for estimating and compensating it in the circular and spiral signals, for different SNR, multipath spreads and doppler factors.

VI. Acknowledgement

We would like to thank the City Council of Loulé, namely to its President Vítor Aleixo and Mr. Pedro Gema, for providing the use of the Loulé City Pools to carryout the acoustic experiments.

This work was supported by LARSyS funding (DOI: 10.54499/LA/P/0083/2020, 10.54499/UIDP/50009/2020, and 10.54499/UIDB/50009/2020).

Rúben S. Viegas is supported by the grant 2023.03744.BD from the Portuguese Foundation for Science and Technology (FCT).

References

[1] B. R. Dzikowicz, B. T. Hefner, and R. A. Leasko, "Underwater acoustic navigation using a beacon with a spiral wave front," *IEEE Journal of Oceanic Engineering*, vol. 40, no. 1, pp. 177–186, 1 2015.

[2] B. R. Dzikowicz, J. Y. Yoritomo, J. T. Heddings, B. T. Hefner, D. A. Brown, and C. L. Bachand, "Demonstration of spiral wavefront navigation on an unmanned underwater vehicle," *IEEE Journal of Oceanic Engineering*, pp. 1–10, 2023.

[3] B. R. Dzikowicz, J. F. Tressler, and D. A. Brown, "Demonstration of spiral wave front sonar for active localization," *The Journal of the Acoustical Society of America*, vol. 146, no. 6, pp. 4821–4830, 12 2019.

[4] A. Munafo, J. Sliwka, G. Ferri, A. Vermeij, R. Goldhahn, K. LePage, J. Alves, and J. Potter, "Enhancing AUV localization using underwater acoustic sensor networks: Results in long baseline navigation from the COLLAB13 sea trial," in *2014 Oceans - St. John's*. IEEE, 9 2014.

[5] C. Militello and S. R. Buenafuente, "An exact noniterative linear method for locating sources based on measuring receiver arrival times," *The Journal of the Acoustical Society of America*, vol. 121, no. 6, p. 3595, 2007.

[6] N. R. Rypkema, E. M. Fischel, and H. Schmidt, "Closed-loop single-beacon passive acoustic navigation for low-cost autonomous underwater vehicles," in *2018 IEEE/RSJ International Conference on Intelligent Robots and Systems (IROS)*. IEEE, 10 2018.

[7] L. Paull, S. Saeedi, M. Seto, and H. Li, "AUV navigation and localization: A review," *IEEE Journal of Oceanic Engineering*, vol. 39, no. 1, pp. 131–149, 2014.

[8] X. Su, I. Ullah, X. Liu, and D. Choi, "A review of underwater localization techniques, algorithms, and challenges," *Journal of Sensors*, vol. 2020, pp. 1–24, 2020.

[9] S. Sun, T. Liu, Y. Wang, G. Zhang, K. Liu, and Y. Wang, "High-rate underwater acoustic localization based on the decision tree," *IEEE Transactions on Geoscience and Remote Sensing*, vol. 60, pp. 1–12, 2022.

[10] R. Viegas, F. Zabel, and A. J. Silva, "In-lab demonstration of an underwater acoustic spiral source," *Sensors*, vol. 23, no. 10, p. 4931, May 2023.

[11] B. R. Dzikowicz and B. T. Hefner, "A spiral wave front beacon for underwater navigation: Transducer prototypes and testing," *The Journal of the Acoustical Society of America*, vol. 131, no. 5, pp. 3748–3754, 5 2012.

[12] D. A. Brown, B. Aronov, and C. Bachand, "Cylindrical transducer for producing an acoustic spiral wave for underwater navigation (l)," *The Journal of the Acoustical Society of America*, vol. 132, no. 6, pp. 3611–3613, 12 2012.

[13] W. Lu, Y. Lan, R. Guo, Q. Zhang, S. Li, and T. Zhou, "Spiral sound wave transducer based on the longitudinal vibration," *Sensors*, vol. 18, no. 11, p. 3674, 10 2018.

[14] W. Lu, R. Guo, Y. Lan, H. Sun, S. Li, and T. Zhou, "Underwater spiral wave sound source based on phased array with three transducers," *Sensors*, vol. 19, no. 14, p. 3192, 7 2019.

[15] B. T. Hefner and B. R. Dzikowicz, "A spiral wave front beacon for underwater navigation: Basic concept and modeling," *The Journal of the Acoustical Society of America*, vol. 129, no. 6, pp. 3630–3639, 6 2011.

[16] R. Viegas, F. Zabel, and A. J. Silva, "Underwater acoustic spiral source: pool tests and calibration," in *OCEANS 2023 - Limerick*. IEEE, Jun. 2023.